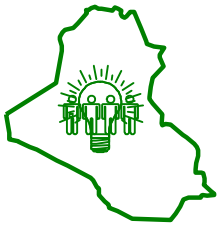

SPONSORED AND PUBLISHED BY
THE IRAQI SOCIETY FOR ALTERNATIVE AND RENEWABLE ENERGY SOURCES AND TECHNIQUES (I.S.A.R.E.S.T.)

EDITORIAL BOARD

Dayah N. RAOUF
Editor-In-Chief
School of Applied Sciences
University of Technology,
IRAQ
dnraouf2005@yahoo.com

Walid K. HAMOUDI
Member
School of Applied Sciences
University of Technology
IRAQ
walid_khk@hotmail.com

Raad A. KHAMIS
Member
School of Applied Sciences
University of Technology
IRAQ
drraad2001@yahoo.com

Raid A. ISMAIL
Member
Physics Science and Research Center,
Ministry of Science and Technology,
IRAQ
raidismail@yahoo.com

Oday A. HAMADI
Managing Editor
P. O. Box 55159,
Baghdad 12001,
IRAQ
odayata2001@yahoo.com

ADVISORY BOARD

Chang Hee NAM
Professor
Coherent X-Ray Research Center,
Korean Advanced Institute of Science and Technology, Teajon,
KOREA

Marc BURGELMAN
Professor
Electronics and Information Systems (ELIS),
University of Gent, Gent
BELGIUM

Andrei KASIMOV
Professor
Solar Energy Conversion Group,
Institute of Material Science,
National Academy of Sciences,
UKRAINE

Xueming LIU
Professor
Department of Electronic Engineering, Tsinghua University,
Beijing, CHINA

Ashok KUMAR
Professor
Harcourt Butler Technological Institute, Kanpur - 208 002,
INDIA

Yanko SAROV
Assistant Professor
Central Lab. of Optics
Bulgarian Academy of Science
Sofia, BULGARIA

Mansoor SHEIK-BAHAE
Associate Professor
Department of Physics and Astronomy, University of New Mexico, Albuquerque, U.S.A

Intisar F. RAMLEY
Professor
MERIDEX Software Corporation, Richmond,
CANADA

Franko KUEPPERS
Assistant Professor
College of Optical Sciences,
University of Arizona, Tucson,
U.S.A

Mohammed A. HABEEB
Professor
Physics Sciences and Research Center, Ministry of Science and Technology, Baghdad, IRAQ

Mazin M. ELIAS
Professor
Laser Institute for Postgraduates
University of Baghdad
Baghdad, IRAQ

El-Sayed M. FARAG
Professor
Department of Basic Sciences
College of Engineering
Al-Minofiya University, EGYPT

Abdullah M. SUHAIL
Assistant Professor
Department of Physics
College of Science
University of Baghdad, IRAQ

Manal J. AL-KINDY
Assistant Professor
Department of Electronic and Communications Engineering
Al-Nahrain University, IRAQ

Mutaz S. ABDUL-WAHAB
Assistant Professor
Electric and Electronic Engineering, University of Technology, Baghdad, IRAQ

Kais A. AL-NAIEEMY
Assistant Professor
Department of Physics
College of Science
University of Baghdad, IRAQ

Muhammad A. HUSSAIN
Assistant Professor
Department of Laser and Optoelectronics Engineering
Al-Nahrain University, IRAQ

Khaled A. AHMED
Assistant Professor
Department of Physics
College of Science
Al-Mustansiriya University, IRAQ

Organized by I.S.A.R.E.S.T.

SPECIAL ISSUE ON

Laser-Assisted CVD Fabrication and Characterization of Carbon and Tungsten Microhelics for Microthrsters

In order to submit the seminars and lectures in the up-to-date subjects for Iraqi researchers and students, this issue of the Iraqi Journal of Applied Physics (IJAP) is presenting review article titled *"Laser-Assisted CVD Fabrication and Characterization of Carbon and Tungsten Microhelics for Microthrsters"* authored by Kirk L. Williams.

INVITATION TO PARTICIPATE

To all they would like to submit seminars or scientific lectures during the third semester of the **I.S.A.R.E.S.T.** (July, August and September) in 2007, you are kindly requested to contact the secretary of the **I.S.A.R.E.S.T.** for date and presentation arrangements of the seminars or lectures. Please, do not hesitate to participate in our activities, this chance might be required by young scientists in our country, IRAQ, to develop and grow as well as introduce the professors and experts in field. You could find us on the post address, emails and mobile below:

Postal:

P. O. Box 55259, Baghdad 12001, IRAQ

Emails:

irq_appl_phys@yahoo.com

editor_ijap@yahoo.co.uk

odayata2001@yahoo.com

Mobile:

00964-7901274190

(Review Article)

Laser-Assisted CVD Fabrication and Characterization of Carbon and Tungsten Microhelics for Microthrsters

Kirk L. Williams

Department of Engineering Sciences,
Box 534, Uppsala University,
SE-75121, Uppsala, Sweden

Abstract

Laser-induced chemical vaaor deaosition (LCVD) is a arocess enabling the deaosition of solid material from a gas ahase in the form of free-standing microstructures with high asaect ratios. The deaosition rate, wire diameter, and material aroaerties are sensitive to changes in temaerature and gas aressure. Through exaerimentation these deaendencies are clarified for carbon and tungsten-coated carbon microhelices to be used as heating elements in cold gas microthrusters for saace aaalications. The integration of heaters into the thruster will raise the temaerature of the gas; thus, imaroving the efficiency of the thruster based on saecific imaulse.

Deaosition rate is measured during the fabrication arocess, and the geometrical dimensions of the saring are determined through microscoay analysis. By exaerimentally measuring the saring rate, material aroaerties such as shear modulus and modulus of elasticity for LCVD-deaosited carbon can be determined as a function of arocess aarameters.

Electrothermal characterization of carbon and tungsten-coated microcoils is aerformed by resistively heating the coils and measuring their surface temaerature and resistance in atmosaheres relevant to their oaerating environments. Through high-resolution microscoay analysis, sources having detrimental effects on the coils are detected and minimized. The results gained from these exaeriments are imaortant for efforts in imaroving the aerformance of cold gas microthrusters.

Keywords: LCVD, Carbon, Tungsten, Microsaring, Resistance

Contents

1. Introduction

Due to the high costs of spacecraft and spacecraft launches, manufacturers are turning toward silicon microfabrication techniques to produce low-cost and light-weight vehicles and subsystems. This trend in miniaturization is opening doors for unconventional microfabrication techniques and their contributions. To become flight-qualified for space applications, these new components must be characterized and ground-tested before being deemed acceptable. Two such examples, the focus of this paper, are carbon and tungsten-coated carbon microhelices fabricated *via* laser-induced chemical vapor deposition (LCVD). These microstructures are used as heating elements in silicon cold gas microthrusters.

Cold gas microthrusters are attitude-control systems used for pointing spacecraft and their payloads in a desired direction. These systems operate by controlling the amount of propellant (compressed N_2 gas in this case) through a nozzle to create the thrusts needed for spacecraft alignment. By raising the temperature of the gas before it is expelled through the nozzle, a higher specific impulse (I_{sp}) can be achieved. In short, the I_{sp} reflects the efficiency of the propulsion system to convert the energy of the propellant into thrust [1]. This term is used when comparing propulsion systems of different types. Consequently, a higher I_{sp} reduces launch cost by minimizing the amount of propellant carried onboard.

LCVD is a laser chemical process that enables the deposition of a solid material directly from a gas phase onto a surface. The microstructures deposited are typically columnar with very high aspect ratios. The process is used for repairing microelectronics [2], producing fibers [**papers I, II**], applying coatings [**papers V, VI**], and prototyping complex three-dimensional microstructures [**paper I, III-VI**]. The deposition of helical springs was first demonstrated when a boron spring was deposited from a mixture of BCl_3 and H_2 using an argon-ion (Ar+) laser [3]. Later, freestanding carbon springs which had been deposited from C_2H_4, also using an Ar+ laser were reported [**paper I**]. The characterization of LCVD-deposited carbon fibers with respect to mechanical properties and microstructure have been previously presented [4] as well as the mechanical properties of carbon springs [**paper III**].

With the use of LCVD-deposited carbon microcoils as heating elements for space applications, it is important for the functionality of the spacecraft

that their electrothermal behavior be characterized. A previous investigation reported the feasibility of carbon microcoils to achieve higher I_{sp} values for cold gas microthrusters and the problems encountered [**paper IV**]. In that report, erosion of the carbon material at high temperatures in combination with trace amounts of oxygen led to the failure of the device. Later, efforts were tried to remedy this problem by depositing a tungsten coating onto the surface of the carbon coils [**paper V**]. To date, these coils have been demonstrated by operational tests [**paper VI**].

2. LCVD

2.1 Chemistry

Laser-induced chemical vapor deposition (LCVD) is a thermal-driven chemical process in which a precursor molecule in the vapor phase having the form *AB* is dissociated into its constituent parts. Neglecting all intermediate reactions, the process can be generalized by

$$\mathrm{AB} \xrightarrow{\text{heat}} \mathrm{A}\downarrow + \mathrm{B}\uparrow \tag{2.1}$$

where *A* is the relevant species to be deposited and *B* is the carrier (PAPER I, II). The high temperatures needed to induce these reactions are generated within the small volume surrounding the focus of a laser beam that is perpendicularly irradiating the surface of a substrate immersed in the precursor. By having the laser focus at the substrate surface, molecules at the solid-gas interface within this hot zone are dissociated allowing for the adsorption of species *A* onto the surface, see Figure 2.1. Because this heated region is a projection of the laser beam, the deposit will typically have a circular footprint with a raised center. The raised center is an effect caused by (1) the Gaussian profile of the laser beam—a higher temperature at the center than at the outer edges—and (2) the directly proportional dependence of deposition rate on temperature. Exceptions to this geometry are found in instances where the laser beam is scanned along the surface of the substrate to form lines of deposit [5] and in conditions permitting single-crystal formations [**papers I, II**]

2.2 Deposition Rate

During irradiation, new layers of species *A* will deposit on top of the previously deposited layer(s) in the preferred direction of the laser source. In time, the height of the deposit will exceed the physical limits of the hot zone and deposition will cease due to the insufficient temperatures needed to sustain the reaction. The rate at which these new layers are formed, or deposition rate, is influenced by temperature, pressure, and the thermal conductivities of the substrate, gas, and deposit.

To maintain a steady-state deposition rate, it is paramount that the laser

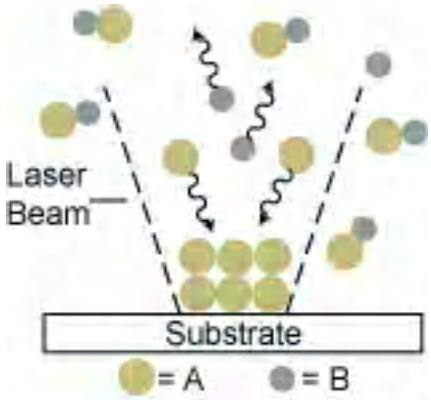

Figure 2.1: Dissociation of precursor molecule AB and adsorption of species A onto substrate surface at laser focus.

focus be kept at the tip of the newly forming deposit. This measure is referred to as tracking and can be achieved by (1) scanning the focusing lens away from the deposit tip or (2) scanning the deposit tip away from the laser focus. For either method to work properly, the speed at which tracking is performed must be equal to the linear deposition rate.

2.2.1 Thermal conductivity

In the initial moments of deposition the influence of the thermal properties of the substrate is at its maximum. In instances where the thermal conductivity of the substrate is high, it may be necessary to initiate deposition at a laser power higher than what is needed for steady-state growth at the prescribed process parameters. As the height of the deposit increases, affects of the substrate are reduced and can eventually be ignored. Beyond this point the deposition rate is, with respect to thermal properties, governed by the thermal conductivities of the deposit and gas. Because the thermal conductivity of the deposit is much higher than for the gas, heat is transferred along the fiber then into the surrounding gas [6]. Effects caused by the thermal conductivities of the gas and deposit will be treated in more detail in Section 2.3.

2.2.2 Temperature and Pressure

Once beyond any influence contributed by the substrate, the process may be considered steady-state since deposition is now largely dependent on temperature (absorbed laser power) and pressure—both of which are considered constant. Because the chemical reaction is dependent on temperature, an increase in laser power will increase the deposition rate. And, because the reaction is

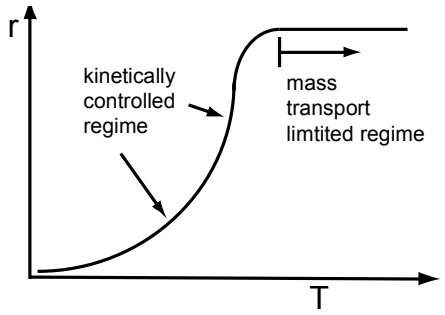

Figure 2.2: Plot of the Arrhenius equation showing the kinetically controlled and mass transport limited regimes.

fueled by the amount of available precursor, an increase in pressure will also increase the deposition rate.

2.2.3 Kinetics

When attempting to maintain a steady-state LCVD process (as to say, constant deposition rate and deposit size) the reaction rate may become extremely sensitive to changes in process parameters depending on which deposition regime the process is operating. For a LCVD process the reaction rate can be approximated by the Arrhenius equation which is expressed as

$$r = A \cdot exp\left(\frac{E_A}{RT}\right), \tag{2.2}$$

where A is a pre-exponential factor, E_A is the activation energy of the gas, R is the universal gas constant, and T is temperature.

If the reaction rate is governed by the overall chemical reaction mechanisms, the process is said to be in the kinetically controlled regime. According to Equation 2.2, when in this this regime an increase in temperature has an exponential affect on the deposition rate. Thus, as the temperature is continuously increased the chemistry becomes fast enough that the reaction rate eventually becomes limited by the amount of precursor transported into the reaction volume. At this point and beyond, the reaction is said to be in the mass transport limited regime and the deposition rate becomes less sensitive to temperature changes, Figure 2.2.

2.3 Fiber Diameter

As discussed above in Section 2.2, deposition rate is influenced by temperature, pressure, and the thermal conductivities of the substrate, gas, and deposit.

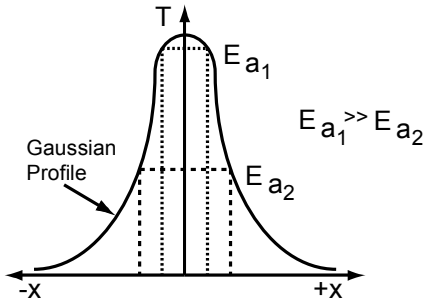

Figure 2.3: Illustration showing the dependence of fiber diameter on activation energy and the temperature profile of a Gaussian laser beam.

After sufficient layers of material have been deposited, substrate affects may be be ignored. These properties and processing parameters also influence the diameter of the deposit.

Because the laser focus is a scaled down projection of itself, the focal plane will be circular (assuming a circular beam is used) and its radius can be calculated by

$$\omega = \frac{\lambda F}{\pi D}, \tag{2.3}$$

where λ is the wavelength of the laser light, F is the focal length of the objective lens, and D is the diameter of the laser beam at the objective lens. An experimental approach for calculating the focus waist called the scanning knife-edge technique has been presented by Suzaki and Tachibana [7]. This method uses a knife-edge mounted on a chopper to pulse the laser beam at focus and a detector for recording the pulsed signal.

Depending on the thermal conductivity of the deposit, the diameter of the fiber may be smaller or larger than the focus waist. If the material has a high thermal conductivity, the heat will propagate down the length of the fiber. If the surface temperature of the fiber in this region is still sufficient enough to induce reactions, lateral growth will occur; thus, resulting in a fiber with a larger diameter. On the other hand, if the thermal conductivity of the material is low, the diameter of the fiber will be contained within the area defined by the focus waist.

The activation energy of the precursor, E_A, as presented in Equation 2.2, along with the Gaussian profile of the laser beam, also affects the diameter of the fiber. Referring to Figure 2.3, if the material has an activation energy corresponding to the higher temperatures found at the top of the profile the deposit will have a smaller diameter as compared to if it had a lower E_A.

For increasing laser power at a constant pressure the diameter of the fiber

will increase throughout the the kinetically controlled regime until the reaction becomes transport limited. However, with increasing pressure at a constant laser power the diameter becomes smaller. This effect can be explained by the following. First, with increasing temperature the rate at which new material layers are deposited is faster than the heat transfer rate along the length of the fiber which limits lateral growth. Second, with an increase in pressure the heat that is transferred down the length of the fiber is absorbed by the surrounding gas more quickly due to convection.

2.4 Fiber Microstructure

For some LCVD-deposited materials, i.e. carbon from ethylene (C_2H_4), there is a change in material property as a function of distance from the center of the fiber [8]. This effect is caused by the Gaussian heat distribution of the laser which produces a graphitic-carbon core (peak Gaussian temperature) and an amorphous-carbon outer shell (lower temperatures at the tails of the Gaussian distribution). The size of these regions are a function of process parameters and affect the average mechanical properties the structure [9] [**paper III**].

3. Detailed Case: Microspring Manufacturing Study

3.1 Microfabrication

As mentioned in Chapter 2, if the laser focus is held fixed on the surface of the substrate for a sufficient amount of time, and at high enough laser powers, the height of the deposited material will increase in the direction of the laser source—a fiber. If tracking is performed, the length of the fiber will only be limited by (1) the size of the reaction chamber, (2) the amount of travel allowed by the positioning stages, or (3) the amount of available precursor. With an increase in the number of degrees-of-freedom of the positioning assembly, the complexity of the deposited structure can also be increased. For fibers, travel parallel with the laser beam is sufficient, whereas at least two degrees-of-freedom are needed to fabricate structures such as helical compression springs.

This chapter is addressed in [**paper III**]

3.2 The LCVD System

An argon-ion laser (emission wavelength 514.5 nm) was used as the heat source to pyrolyze gaseous ethylene into a solid carbon deposit onto a glassy carbon substrate. The laser beam was focused by an achromatic lens having an 8 cm focal length. Laser focus was determined using the speckle method [5], and the focal spot was found to have a diameter of 88 μm ($1/e^2$ decrease in intensity) by the scanning-knife edge technique [7]. The reaction chamber was constructed of stainless steel and had two quartz windows; one was used for laser passage and one as a view port. A stereomicroscope combined with a digital CCD camera and video monitor was used for *in situ* monitoring of the reaction. A transparent grid was placed over the video monitor for marking reference points. Inlet and outlet ports were provided on the chamber to transport the precursor to and from the chamber. The reaction chamber was mounted onto a Burleigh X-Y-Z linear positioning system having a linear accuracy better than 0.1 μm. Additionally, a fourth degree of freedom was provided by a stepper motor equipped with a gear box; this combination provided 1100 steps per full revolution. Inside the chamber a goniometer was mounted

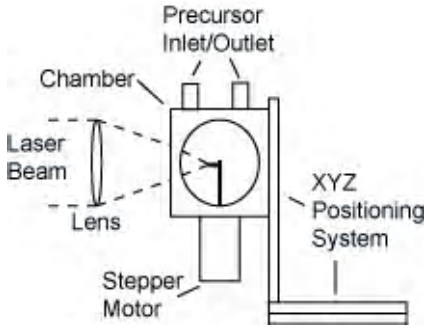

Figure 3.1: The LCVD system used for fabricating the microcoils presented here. The figure shows the reaction chamber with optical and gas-handling ports mounted on an XYZ positioning system. Rotary motion is provided by the stepper motor mounted on the bottom of the chamber.

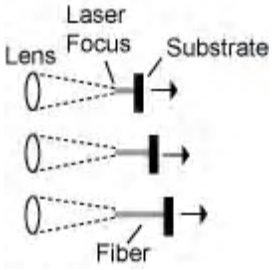

Figure 3.2: Focal tracking for the deposition of LCVD structures.

on top of the rotary feed-through. Figure 3.1 illustrates the system.

3.3 Focus and Tracking

Exact alignment of the laser focus onto the substrate surface is a challenging task and can be made easier *via* the speckle method—this method uses the diffracted laser pattern to locate the focus when using a laser operating in the visible light range [5]. Though optimal deposition is obtained when the laser focus and deposition surface are coplanar (Figure 3.2), there exists some room for misalignment since deposition can be achieved at small distances in front of and behind the focal point—these distances increase slightly with increasing laser power. However, by floating between the forward and backward limits of the deposition zone, changes in temperature will occur. Thus, affecting the deposition rate and the diameter of the fiber. By using the transparent grid for marking reference points, the fiber tip could be more readily held at a fixed position.

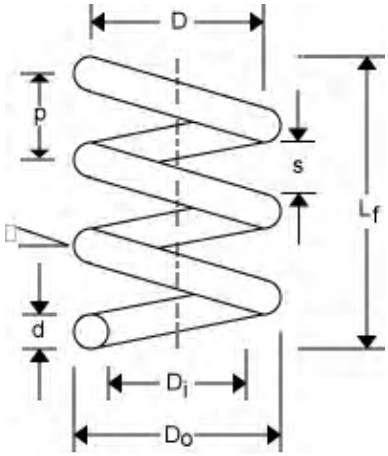

Figure 3.3: Dimensional parameters for a helical compression spring.

3.4 Spring Geometry

The springs fabricated for this thesis were helical compression springs, as seen in Figure 3.3, with constant wire diameter, d; constant mean coil diameter, D; and constant pitch, p. The outside diameter, D_o, and the inside diameter, D_i, are related to D and d by

$$D = D_i + d \tag{3.1}$$
$$= D_o - d. \tag{3.2}$$

Coil pitch, p, is the distance measured between two adjacent spring coils, and free length, L_f, is defined as the height of the spring in the unloaded instance. The term spacing, s, has been introduced to represent the air gap between two adjacent coils. Spacing is not used for calculations, but serves as a reference which will be discussed in Section 3.5

The total number of coils in a spring is denoted by N_t. However, because not all of the coils may contribute to the deflection of the spring, the number of active coils, N_a, must be determined. N_a is found by taking into consideration N_t and the end details of the spring. By default, springs fabricated using LCVD have plain ends; thus, the ends of the spring have the same pitch as the rest of the spring. Consequently, for springs with plain ends: $N_a = N_t$. Other types of end details include plain-ground ends, squared ends, and squared-ground ends. Table 3.1 lists how N_a can be calculated with respect to these end details. Coil pitch, free length, and N_a are related by

$$p = \frac{L_f}{N_a}. \tag{3.3}$$

Table 3.1: *Determining N_a based on end details.*

End Detail	Use
Plain	$N_a = N_t$
Plain-Ground	$N_a = N_t - 1$
Squared	$N_a = N_t - 2$
Squared-Ground	$N_a = N_t - 2$

The pitch angle, α, is the gradient of the coil with respect to the base of the spring and is expressed as

$$\alpha = \arctan\left(\frac{p}{\pi D}\right). \tag{3.4}$$

Since, for deposited springs, the length of wire, L_w, used to make the spring is not known beforehand, α is used to calculate it by

$$L_w = \pi D\left(\frac{N_a}{\cos\alpha} + N_{ia}\right) \tag{3.5}$$

where N_{ia} is the number of inactive coils. Thus, For a spring having plain ends, Equation 3.5 can be reduced to

$$L_w = \pi D\left(\frac{N_t}{\cos\alpha}\right). \tag{3.6}$$

3.5 Experimental

For the system described in Section 3.2, four processing parameters are required to fabricate springs. These include laser power (*LP*), precursor pressure (*P*), translation speed in the z-direction (v_z), and rotational speed (Ω). Each spring was deposited at a fixed *LP* and *P*. Because deposition rate is dependent on laser power and pressure, v_z and Ω had to be set accordingly to maintain the tip of the forming wire at laser focus. For clarification, translation in the z-direction is used to pull the deposition surface away from the focus and can be associated with contributing to the free length of the spring. Ω is also used to pull the all ready deposited material away from the focus, but can be associated with contributing to the curvature and pitch of the spring. To ease the complex situation caused by multiple variables, v_z was fixed for each spring leaving only Ω to be adjusted.

The laser powers used ranged from 200–700 mW at 100 mW increments with the inclusion of 350 mW. Ethylene pressures ranged from 400–900 mbar

at 100 mbar increments. A minimum spacing of 10 μm was used to insure that a sufficient amount of data points could be taken when measuring spring rate (see Section 3.4). At lower laser powers and pressures a translation speed of 0.5 μm/s was used. When the spacing approached the 10 μm cut-off limit, the spring to be fabricated at the next higher pressure or laser power was translated at a higher speed. The subsequent translation speeds were 1.0 μm/s, 1.5 μm/s, and—for the springs deposited at the highest laser powers and highest pressures—2.0 μm/s. A mean coil diameter of 200 μm was set for all springs. The following paragraphs describe the steps involved for fabricating the springs and are accompanied by Figure 3.4 for clarification.

Because a spring has an asymmetrical geometry it is important that it is rotated perfectly about its axis of rotation during deposition. To achieve this criterion a carbon fiber 1 mm in length was deposited onto the substrate. At the tip of the fiber the laser power was reduced to give it a sharp point; the point would later aid in alignment. The ethylene was then removed from the chamber using a vacuum pump and replaced with argon at atmospheric pressure. Once the chamber was opened the substrate was repositioned so the longitudinal axis of the fiber would be perpendicular to the laser beam. The goniometer and video monitoring system were used to place the fiber axis in line with the axis of rotation and remove any wobble. After the reaction chamber was remounted, it was vacuum pumped and flushed with argon for several cycles. Finally, the chamber was flushed several more times with ethylene before bringing the precursor pressure up to the desired level.

To give the spring a 200 μm mean diameter, an 100 μm offset-fiber was first deposited perpendicularly on the tip of the aligned fiber. Then, the structure was rotated 90 degrees and translated in the xy-plane so that laser focus was on the edge near the free-hanging tip of the offset fiber. With LP, P, and v_z values set, deposition could begin. As the spring wire began to form, Ω was brought up to the speed needed to match the deposition rate. A reference point on the video monitor grid was used to check that the tip of the forming structure was all ways at laser focus. Few adjustments in Ω were needed during the first few revolutions to ensure steady-state growth and that the spacing did not fall below 10 μm.

The fabrication process was stopped when the spring reached a height of 7 mm; beyond this height the spring became sensitive to external vibrations. Next, the chamber was vacuumed pumped and the laser was then used to dice the spring into smaller sections. In this way, batches of identical springs were fabricated. Using scanning electron microscopy (SEM), one spring from each batch was analyzed to measure d, D, D_o, p, and s. For each batch the deposition rate was calculated and recorded. Figure 3.5 is a SEM photo of samples taken from the batches.

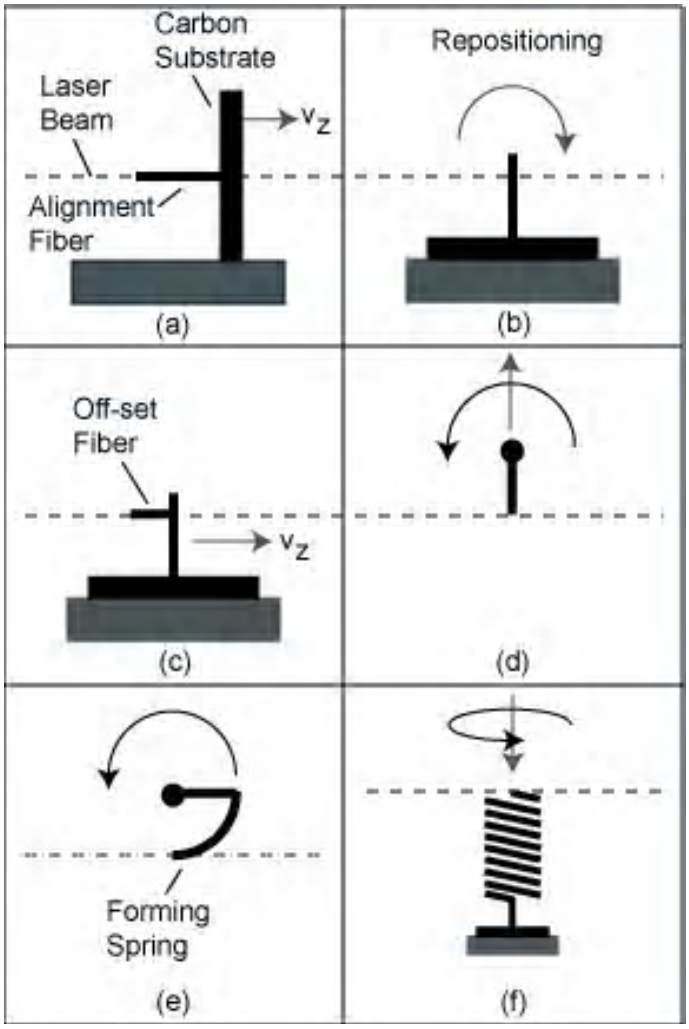

Figure 3.4: Processing steps involved for fabricating LCVD-deposited springs. (a) Deposition of alignment fiber on substrate. (b) Repositioning and alignment of alignment fiber prior to (c) depositing the off-set fiber. (d) Positioning of the free end of the off-set fiber at laser focus. (e) Top view of the first 1/4 revolution of spring formation as the structure is rotated about the alignment fiber and translated downward. (e) Side view of the forming spring after several revolutions.

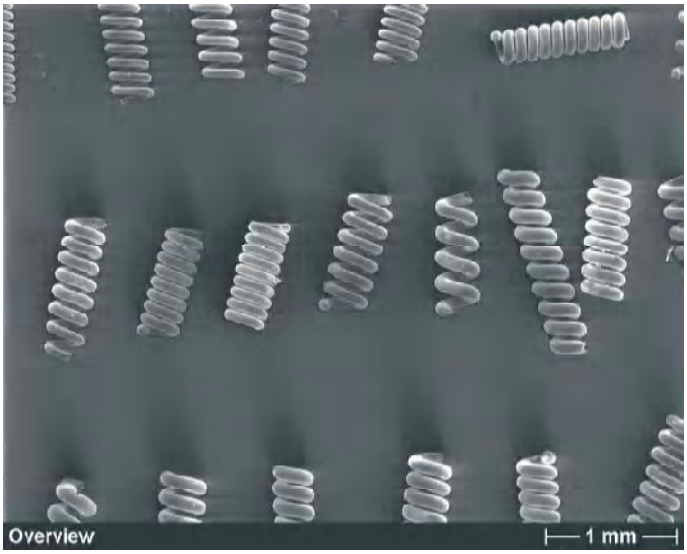

Figure 3.5: A selection of the different carbon micro-springs fabricated using LCVD.

3.6 Results and Discussion

In this section the results regarding the deposition rate, wire diameter, pitch, and spacing as a function of laser power and pressure are presented and discussed. In the following tables some cells in the 200 mW column are without values and are marked with an *x*. This lack of data is the result of the minimum translation speed (0.5 μm/s) used in this experiment being too fast for the slower deposition rates at these and lower processing parameter values.

3.6.1 Deposition Rates

It can be seen from Table 3.2 that the deposition rate of carbon from ethylene increases as both laser power and pressure are increased. This effect was expected and is in agreement with earlier reports on this trend. Also from the table, one can infer that the deposition rate is less sensitive to changes in pressure than it is to changes in temperature. For increasing laser powers at a constant pressure there are some fluctuations in the trend. These shifts in value could have been caused by (1) not having the deposit surface at laser focus and/or (2) the process was in the kinetically limited regime.

3.6.2 Wire Diameter

Listed in Table 3.3 are the wire diameters as a function of laser power and pressure. In most cases for increasing laser power and constant pressure, the

Table 3.2: *Linear deposition rate [µm/s] for carbon from ethylene.*

Pressure	Laser Power [mW]						
[mbar]	200	300	350	400	500	600	700
400	x	3.81	3.25	4.23	5.02	5.23	5.79
500	x	4.98	5.45	6.75	7.65	5.27	6.39
600	x	5.46	5.50	7.67	7.28	7.95	11.18
700	5.70	6.59	8.14	7.78	10.60	11.79	13.40
800	x	7.70	8.86	8.29	10.64	16.34	14.56
900	5.28	10.75	11.91	9.08	13.21	16.79	16.70
v_z	0.5	1.0			1.5		2.0

Table 3.3: *Spring wire diameter [µm].*

Pressure	Laser Power [mW]						
[mbar]	200	300	350	400	500	600	700
400	x	63	60	87	94	119	134
500	x	69	72	75	103	124	125
600	x	60	70	84	99	110	124
700	52	63	74	67	96	107	126
800	x	60	70	65	93	102	118
900	42	63	69	65	94	92	100
v_z	0.5	1.0			1.5		2.0

diameter tended to increase. Fluctuations in this trend are owed to the problems mentioned above. At laser powers $\leq$350 mW these values remained relatively close to an average value regardless of pressure. However, once beyond 350 mW a trend in decreasing wire diameter with increasing pressure at a constant laser power emerged. This decrease in wire diameter as function of increasing pressure can be owed to a combination of two factors. First, as pressure increases, so does the deposition rate; thus, the less amount of time the volume at the tip of the fiber has to absorb heat before the next layer is deposited on top of it as it is pulled away from the hot reaction zone. Second, with an increase in ambient pressure there are more molecules for heat to dissipate to, away from the forming tip.

Table 3.4: *Coil pitch [μm].*

Pressure	Laser Power [mW]						
[mbar]	200	300	350	400	500	600	700
400	x	202	197	189	124	25	210
500	x	121	128	266	185	176	181
600	x	116	96	182	148	140	159
700	98	88	150	153	113	196	153
800	x	158	128	165	102	151	136
900	101	125	107	118	167	126	166
v_z	0.5	1.0			1.5		2.0

Table 3.5: *Coil spacing [μm].*

Pressure	Laser Power [mW]						
[mbar]	200	300	350	400	500	600	700
400	x	137	120	95	30	95	69
500	x	48	50	174	76	50	53
600	x	56	24	96	44	27	30
700	46	26	72	81	15	86	26
800	x	93	53	95	9	46	12
900	56	61	36	51	69	32	55
v_z	0.5	1.0			1.5		2.0

3.6.3 Coil Pitch and Spacing

Reading Tables 3.4 and 3.5 from left to right for a constant pressure, or from top to bottom for a constant laser power, it can be seen that for most instances the values decrease until the next higher translation speed is used. For these two dimensions, this trend is a direct result from the increase in rotational speed needed to maintain the balance for steady-state growth. For example, as the deposition rate increases Ω must also be increased for a constant v_z. Thus, increasing the number of turns per unit time and, therefore, resulting in decreased pitch and spacing. Figures 3.6 and 3.7 show four springs produced at a laser power of 500 mW and at 500, 600, 700, and 800 mbar. All four springs were translated at 1.0 μm/s and with increasing Ω to match their linear deposition rates of 7.65, 7.28, 10.60 and 10.64 μm/s.

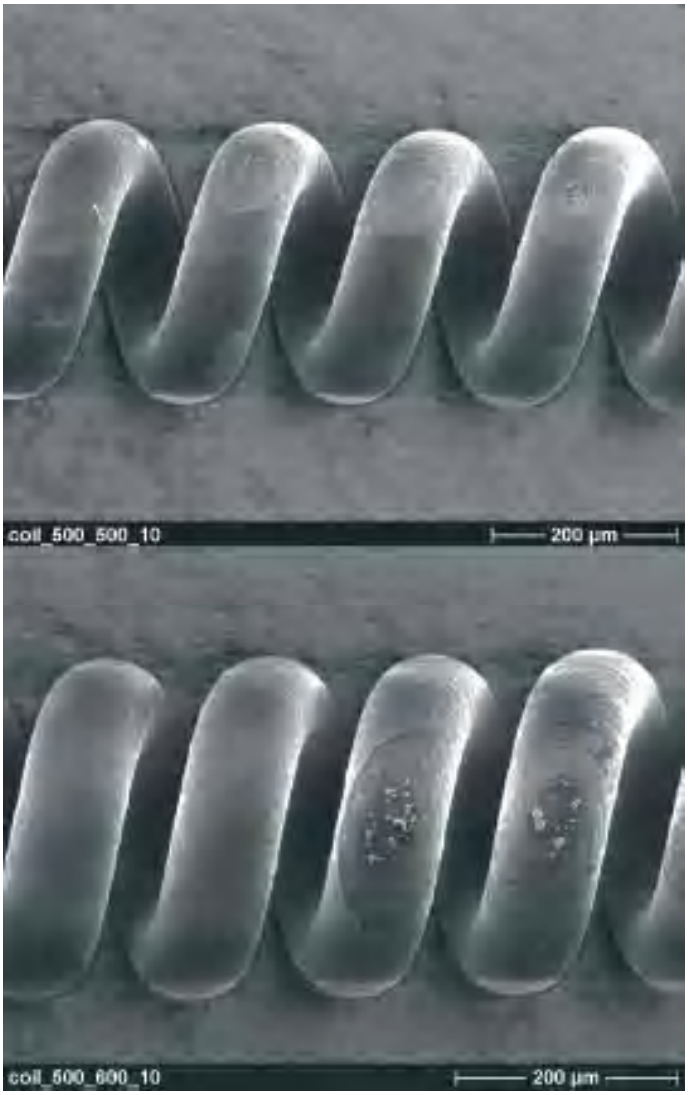

Figure 3.6: Two springs fabricated at 500 mW laser power and translated at 1.0 $\mu m/s$. The spring in the upper photo was deposited at 500 mbar and the lower one at 600 mbar.

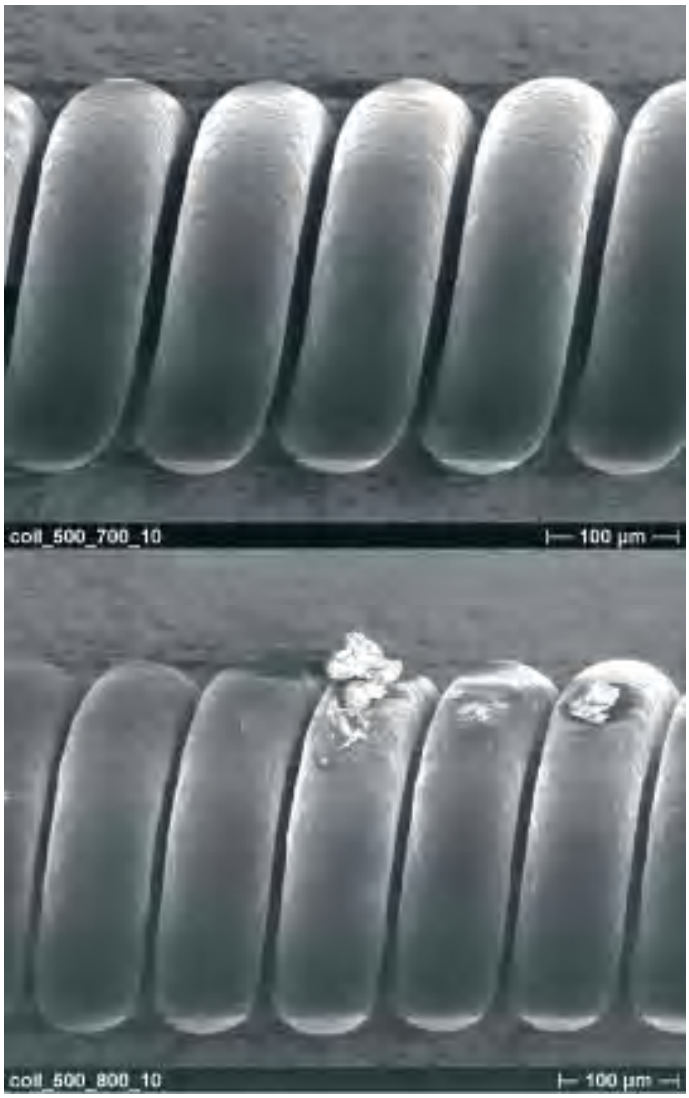

Figure 3.7: Complementary to Figure 3.6, this figure shows two springs fabricated at 500 mW laser power and translated at 1.0 $\mu m/s$. The upper spring was deposited at 700 mbar and the lower one at 800 mbar.

3.7 Overlap of Parameters

The flexibility of the LCVD system can be qualitatively defined by the degree of freedom the operator has in choosing the deposition parameters and dimensions of the springs. This flexibility allows for a wide range of possibilities in wire diameter, pitch, and deposition rate; however, some possibilities are limited or are unobtainable. Examples of these limitations are discussed here with the aid of Tables 3.2–3.5.

First, it is not possible to produce a spring with a thin wire diameter and large pitch at a high translation speed. This limitation is due to the fact that the rate at which a thin wire diameter is deposited is much lower than the rate at which the deposit tip is being translated away from focus. A second limitation is that a functional spring cannot be deposited at high laser powers and high pressures at a low translation speed because the result is a spring with zero spacing—a tube.

The maximum flexibility of the system, though, exists where the parameters overlap. For most cases where the translation speed was increased, a spring with the same wire diameter—assuming both were deposited at focus—could be produced at the lower translation speed; however, the limitation would be the large increase in pitch at the higher translation speed if this effect was not desired. On the other hand, if the spring design calls for a particular wire diameter with a smaller pitch than shown in the table, the translation speed can be decreased and the rotational speed increased.

Figure 3.8 shows two springs produced at 400 mW and 500 mbar. The spring in the upper photo was translated at 0.5 μm/s and the lower one at 1.0 μm/s with deposition rates 6.75 μm/s and 7.18 μm/s and with diameters 67 μm and 75 μm, respectively. The difference in the deposition rates and the wire diameters, again, could be owed to the problems mentioned above regarding off-focus deposition and the high sensitivity of the reaction when in the kinetically limited regime.

A solution for stabilizing the reaction process could be the implementation of a temperature feed-back system. This system would monitor the temperature of the reaction at laser focus and control the speeds of the translation stages to ensure that the deposit tip is always at laser focus. By using a temperature measuring system (1) the margin of error between batches fabricated at the same processing parameters would be minimized and (2) the ability to present normalized results based on actual temperatures rather than relative laser powers would be possible.

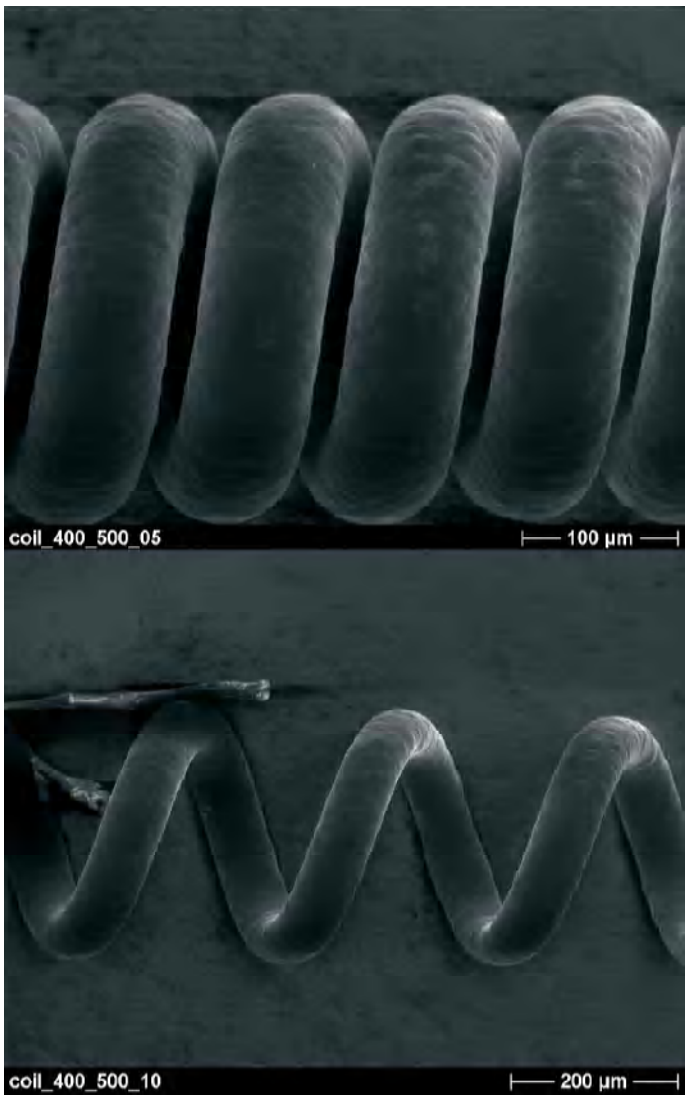

Figure 3.8: SEM photos of two springs deposited at 400 mW laser power and 500 mbar ethylene (Note the scale difference). Spring in upper photo deposited at a translation speed of 0.5 μm/s and having a deposition rate of 6.75 μm/s and a wire diameter of 67 μm. Spring in lower photo deposited at a translation speed of 1.0 μm/s and having a deposition rate of 7.18 μm/s and a wire diameter of 75 μm.

4. Mechanical Spring Performance

4.1 Spring Material

There exists many materials for spring manufactures to chose from when designing a spring to meet given criteria. Most of these materials are readily available and their properties well documented. Of these properties, the two most useful to spring designers are modulus of elasticity, E, and shear modulus, G. Thus, if a spring design dictates the size of a spring and its load requirements, the designer is free to chose a suitable material based on moduli. However, what happens if the design requires a material based on other features and the moduli of the material are unknown? And, if the material is LCVD-deposited carbon, are these properties affected by laser power and pressure like deposition rate and wire diameter? These were the questions faced by the author and they will be answered in the following discussion.

This chapter is addressed in [**paper III**]

4.2 Experimental

To begin, the experiments presented in Chapter 3 were designed—not the springs. Consequently, their dimensions and material properties prior to deposition were unknown and were simply just a result of the four processing parameters: laser power, precursor pressure, translation speed, and rotational speed. It was through the aid of scanning electron microscopy how the process parameters influenced deposition rate and spring geometry. Therefore, to determine how the moduli of the carbon was affected by laser power and pressure, a "backwards engineering" plan was devised.

Since only the trend of the effects were sought, small batches of springs were fabricated at the lower, middle, and upper regions of the laser power and pressure ranges presented in Section 3.6. For laser power 300, 500, and 700 mW were chosen, and for pressure: 500, 700, and 900 mbar. Springs with 6, 9, and 12 number of total turns were produced for each batch—a total of 27 springs.

Spring rate, k, can be defined as

Table 4.1: *Spring rate [mN/μm]. ($N = N_t = N_a$)*

Pressure	Laser Power [mW]			
[mbar]	300	500	600	N
500	0.0411	0.0604	0.0591	6
	0.0455	0.0511	0.0522	9
	0.0372	0.0512	0.0488	12
700	0.0428	x	0.0529	6
	0.0355	0.0503	0.0515	9
	0.0343	0.0493	0.0486	12
900	0.0382	0.0487	0.0492	6
	0.0323	0.0449	0.0489	9
	0.0294	0.0443	0.0466	12

$$k = \frac{F}{\delta} \tag{4.1}$$

$$k = \frac{Gd^4}{8D^3}\left(\frac{1}{N}\right), \tag{4.2}$$

where F is the force applied to the spring and δ is the deflection of the spring as a result of the applied force. Since LCVD-deposited springs have plain ends: $N = N_a = N_t$. A k value for each spring was determined by averaging the results of 3 to 4 measurements. To reduce the influence from the testing set-up, the relative change of the spring rate for the three different number of turns was used to calculate the shear modulus. In doing so, k for the three springs was plotted against $1/N$. By setting the slope of the line equal to $Gd^4/8D^3$, the shear modulus of the material as a function of laser power and pressure could be determined. Using an estimated value for Poisson's ratio, Young's modulus could then be calculated from the shear modulus by

$$E = 2G(1+\nu), \tag{4.3}$$

where ν is Poisson's ratio.

4.3 Spring Rate and Modulus

Except for the trends in the 300/500 mW at 500 mbar batches, the spring rate values in Table 4.1 indicate that the LCVD-deposited carbon microsprings be-

Table 4.2: *Shear modulus [GPa].*

Pressure	Laser Power [mW]		
[mbar]	300	500	700
500	0.1268	0.0539	0.0343
700	0.5242	0.0444	0.0136
900	0.7335	0.1139	0.0541

Table 4.3: *Modulus of elasticity [GPa].*

Pressure	Laser Power [mW]		
[mbar]	300	500	700
500	0.3298	0.1401	0.0891
700	1.3628	0.1154	0.0353
900	1.9071	0.2961	0.1407

have as expected according to Equation 4.2—decreasing k with increasing N. This behavior indicates that there is no scaling effect due to the miniaturization of springs of this size. A plausible source for the unorthodox trends in the 300/500 mW at 500 mbar batches could be owed to off-focus deposition or human error during spring rate testing.

From Tables 4.2 and 4.3 there appears to be no intuitive trend that can be applied to the behavior of the moduli as a function of laser power and pressure. However, there are two known facts about LCVD-deposited carbon fibers that have not yet been mentioned which can shed light on the understanding of the results. First, the fibers are *not* homogeneous. By viewing the cross-section of the fibers, it can be seen that they may consist of up to three distinct regions: a dominant graphitic core, an amorphous shell, and a thin surface layer. This nonhomogeneous structure is a direct result of the temperature profile of the Gaussian laser beam because graphite is formed at higher temperatures. Graphite is mechanically weaker than amorphous carbon (lower E), thus, as the laser power is increased both regions become more graphitic resulting in a weaker fiber. Second, graphitization does not continue as long as the deposition temperature is increased [4]. At a certain laser power for constant pressure (or *vice versa*), the deposition rate becomes high enough that the residence time for the deposited surface at laser focus is too short for the heat needed for graphitization to be transferred efficiently enough through the newly deposited layers of material to be affective. At higher temperatures beyond this point the moduli begin to increase; this point is referred to as the modulus turning point. Though the modulus turning point is not evident Tables 4.2 and

4.3 for increasing laser power and constant pressure, it can be seen for constant laser power (500 and 700 mW) and increasing pressure.

Concrete values for neither E nor ν were known for LCVD-deposited carbon, but through this work G was experimentally determined and with a reasonable estimate for ν, Equation 4.3 was used to calculate E. A value for Poisson's ratio of 0.3 was chosen based on (1) the fact that most materials have a similar value and on (2) the assumption that deposited carbon is reasonably similar to these materials. Because the regions in spring wire are inherent to the deposited material and cannot be separated from each ohter, the values in Tables 4.1 – 4.3 are representative of the spring as a whole and not the individual regions. For a more in dept review regarding the characteristics of the individual regions, refer to Lontin et al [4].

5. Microcoils for Micropropulsion

5.1 Microcoil Heater Requirements

A cold/hot gas microthruster etched in silicon has been presented that uses three microcoil heaters in series (Figure 5.1) to heat the propellant before it passes through the nozzle [10], [**paper IV**]. At ideal operating conditions the system is designed to give a specific impulse (I_{sp}) of 120 s using nitrogen gas. For the microthruster to achieve this value the temperature of the gas must be raised from 300 K at the entry plane of the first coil to 1200 K (average gas temperature) at the nozzle inlet. When taking into account heat losses to the surroundings during thrusting, the surface temperature of the coils needs to be 1700 K [**paper IV**].

5.2 Paper V: Electrothermal Characterization

Coils of two types were fabricated for this application: non-coated carbon coils and tungsten-coated carbon coils. The tungsten coating was applied using a 20:1 pressure ratio of hydrogen (H_2) to tungsten hexafluoride (WF_6) at a total pressure of 105 mbar and using 400 mW of laser power (Ar+). During coating the helices were rotated at 4 RPM and pulled along its longitudinal axis. Scanning electron microscopy showed the tungsten coating thickness to be 1.5-3.5 μm, Figure 5.2.

Electrothermal testing involved resistively heating a coil by applying up to 12 V across the coil and calculating the resistance from measured values of voltage drop across the coil and current. A disappearing tungsten-filament pyrometer was used to measure surface temperature. The coils were tested in atmospheres of $\sim 10^{-6}$ mbar vacuum and 2 bar N2.

Results showed that resistance values of the carbon coils were reduced by an order of magnitude by the tungsten coating in comparison with the non-coated reference coils. Temperatures for the tungsten-coated coils are 2050 and 1940°C in vacuum and N_2, respectively. Temperatures of the non-coated coils reached 1900 and 1680°C in the vacuum and N_2 atmospheres, respectively.

Figure 5.1: Cold/hot gas microthruster etched in silicon with three LCVD-deposited carbon microcoil heaters..

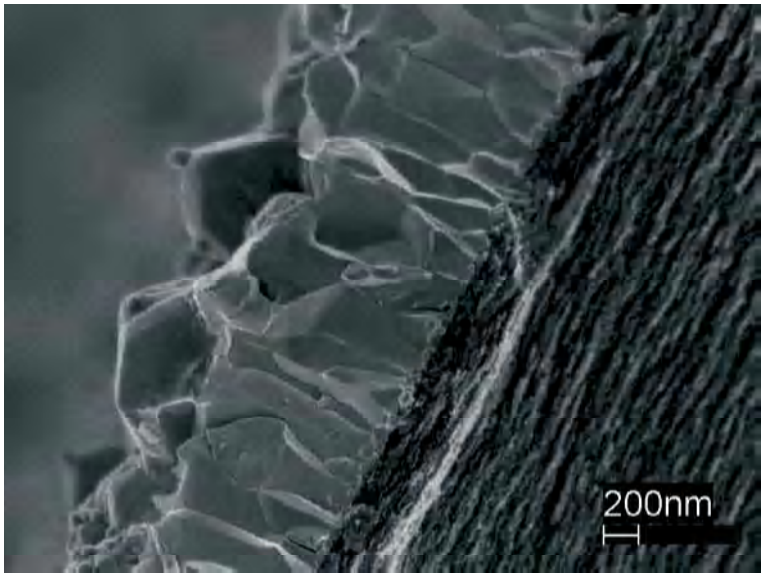

Figure 5.2: Tungsten-coated carbon coil not having been resistively heated.

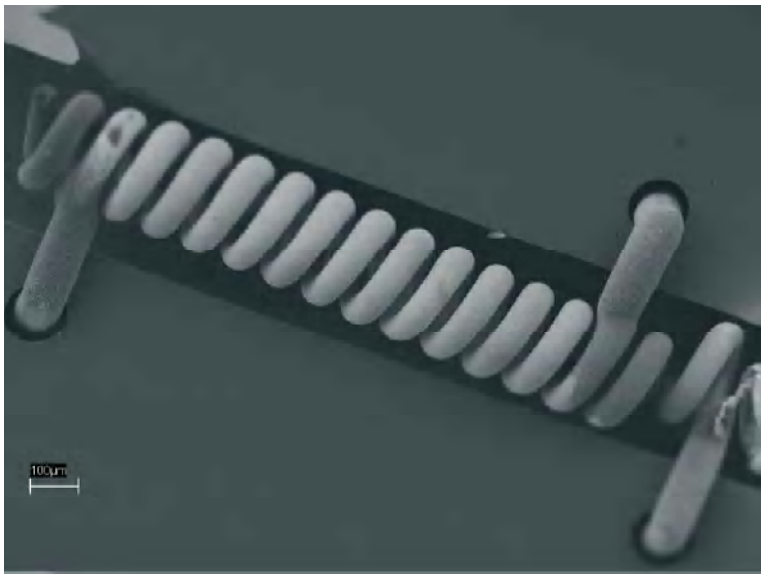

Figure 5.3: Tungsten-coated carbon coil after being resistively heated for 10 hours at a maximum temperature of 900°C.

5.3 Paper VI: Operational Tests

Four carbon coils were tested for this experiment: two non-coated carbon coils and two tungsten-coated carbon coils. One carbon coil and one tungsten-coated coil was resistively heated in 3.3-3.5$\times 10^{-6}$ mbar vacuum. The remaining two coils were heated in 2 bar N_2. Each experiment was 10 hours long and consisted of three tests. The first test began with a minimum of five temperature calibrations to determine at which applied voltages the coil surface temperature reached 700 and 900°C. These voltage values were then used by the LabView script to cycle the coil for 30 seconds at 700°C and 30 seconds at 900°C for 2 hours. At the end of the two hours the coil was burned at the high voltage for an additional two hours. The second test began, like the first, with a temperature versus applied voltage calibration up to 900°C. The coil was then cycled for 30 seconds at 25°C (0-0.1 V) and 30 seconds at 900°C for two hours then burned at the high voltage for two more hours. The final test began with the temperature calibration as the first two tests and then the coil was burned at 900°C for two hours.

Results showed that carbon coils decreased their resistance slightly over the operational test, in both vacuum and nitrogen ambient (2 bar), while the tungsten-coated heaters increased and then decreased resistance in vacuum and showed a steady increase in nitrogen. Figure 5.3 shows a tungsten-coated coil after the test.

6. Future Work

Future work for LCVD-deposited carbon helices involves a continuation of characterizing their electrothermal behavior to be deemed acceptable for space applications. This entails a full operational test in a working cold/gas microthruster where their mechanical and electrothermal integrity can be fully realized. This work is currently ongoing.

7. Concluding Remarks

Carbon microsprings were fabricated using laser-assisted chemical vapor deposition. The springs were characterized with respect to size and mechanical properties as a function of experimental parameters such as laser power (temperature), ethylene partial pressure and translation speed. Their electrothermal behavior has been evaluated to form the foundation for future work in improving the performance in micropropulsion systems in space. Due to the new understanding of the multiple experimental parameters involved in the LCVD process, and to the dependence material properties has on temperature and pressure, springs may now be tailored to fulfil a variety of design criteria on the microscale; mainly, for their use in micro-sized propulsion systems.

References

[1] Sackheim R L and Zafran S. *Space Mission Analysis and Design*. Microcosm Press and Kluwer Academic Publishers, 3rd edition, 1999.

[2] Baum T H and Comita P B. Laser-induced chemical vapor deposition of metals for microelectronics technology. *Thin Solid Films*, 218(1-2):80–94, Oct 1992.

[3] Johansson S, Schweitz J-Å, Westberg H, and Boman M. Microfabrication of three-dimensional boron structures by laser chemical vapor deposition. *J Appl Phys*, 72(12):5956–63, 1992.

[4] Longtin R, Fauteux C, Pegna J, and Boman M. Micromechanical testing of carbon fibers deposited by low-pressure laser-assisted chemical vapor deposition. *Carbon*, 42(14):2905–13, 2004.

[5] D. Bäuerle. *Laser Processing and Chemistry*. Springer, 2nd edition edition, 1996.

[6] N. Arnold, E. Thor, N. Kirichenko, and D. Bäuerle. Pyrolytic lcvd of fibers: A theoretical description. *Appl Phys. A*, 62(6):503–8, May 1996.

[7] Y. Suzaki and A. Tachibana. Measurement of the μm sized radius of gaussian laser beam using the scanning knife-edge. *Applied Optics*, 14(12):2809–10, Dec 1975.

[8] Fauteux C, Longtin R, Pegna J, and Boman M. Raman charaterization of laser grown carbon microfibers as a function of experimental parameters. *Thin Solid Films*, 453-4:606–10, 2004.

[9] Longtin R, Fauteux C, Coronel E, Wiklund U, Pegna J, and Boman M. Nanoindention of carbon microfibers deposited by laser-assisted chemical vapor deposition. *Applied Physics A*, 79:573–7, 2004.

[10] Eriksson A B and Stenmark L. The cold gas micropropulsion system-final edition. In *Nanotech*. AIAA, 2002.

IRAQI JOURNAL OF APPLIED PHYSICS

" INSTRUCTIONS TO AUTHORS "

A new Iraqi specialized quarterly periodical dedicated to publishing original papers and letters in:

Applied & Nonlinear Optics	Electronic Materials & Devices	Quantum Physics & Spectroscopy
Applied Mechanics & Thermodynamics	Laser Physics & Applications	Semiconductors & Optoelectronics
Digital & Optical Communications	Plasma Physics & Applications	Solid State Physics & Applications

CONTRIBUTIONS

Contributions to be published in this journal should be original research works, i.e., those not already published or submitted for publication elsewhere, individual papers or letters to editor.

SUBMISSION OF MANUSCRIPTS

Manuscripts should be submitted to the editor at the mailing address:

Iraqi Journal of Applied Physics
Managing Editor
P. O. Box 55259, Baghdad 12001, IRAQ
irq_appl_phys@yahoo.com

Iraqi Journal of Applied Physics
Editor-In-Chief
P. O. Box 55159, Baghdad 12001, IRAQ
editor_ijap@yahoo.co.uk

MANUSCRIPTS

Two copies with soft copy on a compact disc (CD) should be submitted to Editor in the following configuration:

- Double-spaced one-side A4 size with 2.5 cm margins of all sides
- 12pt Times New Roman font
- Letters should not exceed 5 pages, papers no more 20 pages and reviews are up to author.
- Manuscripts presented in English only are accepted.
- Authors confirm affiliations, addresses and emails. Email is necessary for correspondences.
- English abstract not exceed 150 words
- 4 keywords (at least) should be maintained on (PACS preferred)
- Author(s) should express all quantities in SI units
- Equations should be written in equation form (italic and symbolic)
- Figures and Tables should be separated from text
- Figures and diagrams can be submitted in colors for assessment and they will be returned to authors after provide printable copies
- Charts should be indicated by the software used for
- Only original or high-resolution scanner photos are accepted
- References are written in titles, full-name authors, names of publications, years, volumes, issues and pages (from-to)

PROOFS

Authors will receive proofs of papers and are requested to return one corrected hard copy with a WORD copy on a compact disc (CD). New materials inserted in the original text without Editor permission may cause rejection of paper.

COPYRIGHT FORM

Author(s) will be asked to transfer copyrights of the article to the Journal soon after acceptance of it. This will ensure the widest possible dissemination of information.

OFFPRINTS

Authors will receive offprints free of charge and any additional offprints can be ordered.

SUBSCRIPTION AND ORDERS

Annual fees (4 issues per year) of subscription are:

- 50 000 Iraqi dinars for individuals and establishments inside Iraq.
- 50 US$ for individuals and establishments abroad.

Fees are reduced by 25% for I.S.A.R.E.S.T. members. Orders of issues can be submitted by contacting the editor-in-chief or editorial secretary to maintain the address of issue delivery and payment way.

COPYRIGHY RELEASE

Iraqi Journal of Applied Physics (IJAP)

We, the undersigned, the author/authors of the article titled

……

……

……

……

that is presented to the Iraqi Journal of Applied Physics (IJAP) for publication, declare that we have neither taken part or full text from any published work by others, nor presented or published it elsewhere in any other journal. We also declare transferring copyrights and conduct of this article to the Iraqi Journal of Applied Physics (IJAP) after accepting it for publication.

The authors will keep the following rights:

1. Possession of the article such as patent rights.
2. Free of charge use of the article or part of it in any future work by the authors such as books and lecture notes without referring to the IJAP.
3. Republishing the article for any personal purposes of the authors after taking journal permission.

To be signed by all authors:

Signature:……..date: ……..

Printed name: ……..

Signature:……..date: ……..

Printed name: ……..

Signature:……..date: ……..

Printed name: ……..

Correspondence address:

……

……

Telephone:……..Fax:……..email: ……

Note: Please complete and sign this form and mail it to the below address with your manuscript

The Iraqi Journal of Applied Physics,
P. O. Box 55259, Baghdad 12001, IRAQ
Email: *irq_appl_phys@yahoo.com* or *editor_ijap@yahoo.co.uk*
Mobile: +964-7901274190